

## Article

# Preliminary Forecasting of Rainfall-Induced Shallow Landslides in the Wildfire Burned Areas of Western Greece

Spyridon Lainas, Nikolaos Depountis \*  and Nikolaos Sabatakakis

Department of Geology, Laboratory of Engineering Geology, University of Patras, 265 04 Patras, Greece; splainas@upatras.gr (S.L.); sabatak@upatras.gr (N.S.)

\* Correspondence: ndepountis@upatras.gr; Tel.: +30-210997922

**Abstract:** A new methodology for shallow landslide forecasting in wildfire burned areas is proposed by estimating the annual probability of rainfall threshold exceedance. For this purpose, extensive geological fieldwork was carried out in 122 landslides, which have been periodically activated in Western Greece, after the devastating wildfires that occurred in August 2007 and burned large areas in several parts of Western Greece. In addition, daily rainfall data covering more than 40 years has been collected and statistically processed to estimate the exceedance probability of the rainfall threshold above which these landslides are activated. The objectives of this study are to quantify the magnitude and duration of rainfall above which landslides in burned areas are activated, as well as to introduce a novel methodology on rainfall-induced landslide forecasting. It has been concluded that rainfall-induced landslide annual exceedance probability in the burned areas is higher when cumulative rainfall duration ranges from 6 to 9 days with local differences due to the prevailing geological conditions and landscape characteristics. The proposed methodology can be used as a basis for landslide forecasting in wildfire-affected areas, especially when triggered by rainfall, and can be further developed as a tool for preliminary landslide hazard assessment.

**Keywords:** rainfall threshold; shallow landslides; wildfires; landslide forecasting; landslide hazard



**Citation:** Lainas, S.; Depountis, N.; Sabatakakis, N. Preliminary Forecasting of Rainfall-Induced Shallow Landslides in the Wildfire Burned Areas of Western Greece. *Land* **2021**, *10*, 877. <https://doi.org/10.3390/land10080877>

## Academic Editors:

Domenico Calcaterra, Diego Di Martire, Luigi Guerriero and Roberto Tomás

Received: 20 July 2021

Accepted: 17 August 2021

Published: 20 August 2021

**Publisher's Note:** MDPI stays neutral with regard to jurisdictional claims in published maps and institutional affiliations.



**Copyright:** © 2021 by the authors. Licensee MDPI, Basel, Switzerland. This article is an open access article distributed under the terms and conditions of the Creative Commons Attribution (CC BY) license (<https://creativecommons.org/licenses/by/4.0/>).

## 1. Introduction

Landslides are one of the most frequent and widespread natural disasters around the world, causing a considerable loss in properties and infrastructures. Among all the recognized landslide causal factors, rainfall is widely recognized as the main landslide triggering factor, with mass movement phenomena, such as shallow rotational failures and debris flows. There is an obvious tendency for landslide frequency to increase as rainfall volume or intensity increases. The critical rainfall conditions that may trigger a slope failure at a specific site are dependent on local climate, geological conditions, landslide history, the process of pore water pressure built-up, local morphology, and land-use patterns, as well as the extent of human intervention. The role of each one of the aforementioned causal factors and, most importantly, their combined effect in slope instability is not always pre-defined at the desired scale before a slope failure has occurred. Since landslide prediction is a multidisciplinary task, the examination and analysis of every causal factor at the required scale and detail can aid in a better understanding of the mechanics of landslide initiation, also leading to landslide temporal prediction and forecasting.

Among all approaches of correlating landslide occurrence with rainfall, the concept of “rainfall threshold”, as presented by Caine [1], consists of a commonly used methodology to define the rainfall conditions that, when reached or exceeded, are likely to trigger landslides [2]. Every threshold is based on different climate and geological settings and can be defined under many physical or empirical bases, according to either historical data, statistical or process-based methodologies [3–29].

Most published rainfall thresholds are based on the investigation of rainfall-induced shallow landslides in natural or excavated slopes without the effect of a fire. However, in the

case of recently burned slopes, the processes that facilitate instability are being modified due to the loss of vegetation and the consecutive effects on the upper soil layers, enhancing thus the erosive power of overland flow and resulting in subsequent soil movements [30–36]. Landslides have been documented as occurring either in the first rainy season immediately after the wildfire, from one to two years after the wildfire, or after longer periods [33,37–43].

Recent research on the influence of pine forests root reinforcement decay after fires [44,45] and the consecutive loss of soil strength results show that the reinforcement presented by the roots can be significantly reduced, even four years after the forest fire, due to the degradation of the root's mechanical properties. This means that during the post-fire period, the natural regeneration may not be able to counterbalance the loss of the root reinforcement.

Several studies on the temporal forecasting of landslides [46–48] often aim to create landslide warning systems, usually through real-time monitoring of rainfall data [49–54]. Rainfall thresholds can be fundamental elements for the implementation of landslide forecasting and monitoring. The selection of representative threshold values and the statistical analysis of rainfall events that have resulted in landslides under certain conditions [24,55] can conclude to quantify the likelihood of landslide occurrence as a probability of landsliding within a specific period.

This study uses a proposed empirical rainfall threshold for the possible shallow landslide occurrence in burned areas [56,57] of Western Greece in order to estimate annual probabilities for landslide activation and contribute to shallow landslide forecasting and monitoring in areas of similar conditions. The proposed methodology aims to be developed as a basis for landslide forecasting, especially when triggered by rainfall, also through its application in an area that was affected by a significant natural disaster, and taking into consideration the geological and local conditions of the affected areas.

Given also the unequivocal warming of the climate system, the shifting climate drivers will act on landscapes and slopes that were long modified by human actions and change the current stability status and, in this way, expose more people and areas at higher landslide or flood risk [58,59]. It should be considered that in many areas, e.g., Southern Europe, the mean annual precipitation is projected to remain constant but concentrated in a fewer number of rainy days, resulting in more intense rainfall events, anticipating more frequent shallow landslides [60,61]. A variation in the number of rainy days may result in a variation in the temporal distribution of rainfall-induced landslides and debris flows. In the same areas, the climate models predict a higher air temperature, which will favor evapotranspiration, reducing the amount of water in the sub-surface and increasing the risk of forest fires. To compensate for these challenges, every attempt towards the quantification of the probability of rainfall-induced landslides can be in the near future an important aspect in landslide hazard monitoring and forecasting.

## 2. Methodology

### 2.1. Study Area

The studied area is found in the Ilia Regional Unit, in Western Greece. This area is one of the most well-known and popular archaeological and touristic destinations of Greece because of the archaeological site of Ancient Olympia, the birthplace of the Olympic Games. During the last ten days of August 2007, extensive wildfires burned many regions in the Greek mainland. The total financial loss from the wildfires was estimated to be about 5 billion Euros, classifying this disaster as the worst recorded wildfires in the past 50 years at a national level, and Greece among the countries with the greatest financial damage for 2007.

The Ilia Regional Unit was one of the most affected areas, with approximately 870 km<sup>2</sup> covering approximately 33% of its overall extent. Burned areas included burned rural land (80%), mainly composing of olive trees, pine-tree forests (20%), and villages. The burned areas were extended in a SE-NW direction along with its central parts and were divided into two discrete sections (zones), one at the North (a) and the other at the South

(b) (Figure 1), separated by the valley of the Alfeios river. The Northern burned zone is mainly characterized by agricultural, hilly areas of smooth relief and altitudes up to 800 m, while the Southern has more mountainous and forest terrain, with altitudes up to 1335 m and steeper slopes. The rate of increase in the soil erosion rate on the Northern part of the study area immediately after the wildfire event was found to be equal to 36.2%, with the percentage reducing to 31% after a decade [62]. This is an important circumstance for the study area since soil erosion accelerates landslide occurrence, especially when rainfall infiltrates eroded areas. The soil erosion rate was calculated using the RUSLE equation [63].

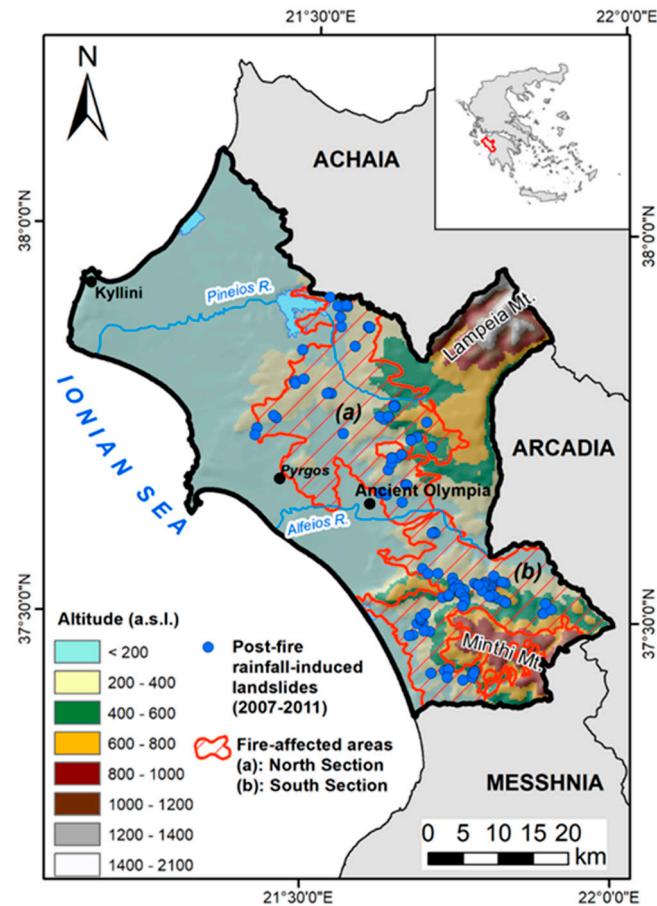


**Figure 1.** Geographical location and post-wildfire landslide inventory of the study area. Hatched areas show the outline of the wildfire-affected areas, divided in Section “a” (North) and Section “b” (South).

## 2.2. Geological Setting

The burned areas consist of Quaternary deposits and post-Miocene (Neogene) sediments overlying the Alpine bedrock. As shown in the simplified regional geological map which has been compiled for the study area (Figure 2), typical geological formations include thick sequences of lacustrine, marine, and fluvial sediments [64,65] such as marls, sandy clays, sandstones, and mudstones, as well as a lower percentage of conglomerates (Figure 3a). Quaternary loose deposits consist of 18.61% and 38.59% of the zones (a) and (b), respectively, while bedrock outcrops range from 28.4% in the South section to only 1.1% in the North zone. Bedrock consists of alpine rock formations belonging to the Olonos-Pindos and Gabrovo Geotectonic units, part of the External Hellenides Orogenetic belt [66]. Main bedrock rock types include typical “flysch-type” sequences of shales, siltstones, and sandstones (Figure 3b), as well as thinly-bedded to massive limestones (Figure 3c), schists, and cherts (Figure 3d).

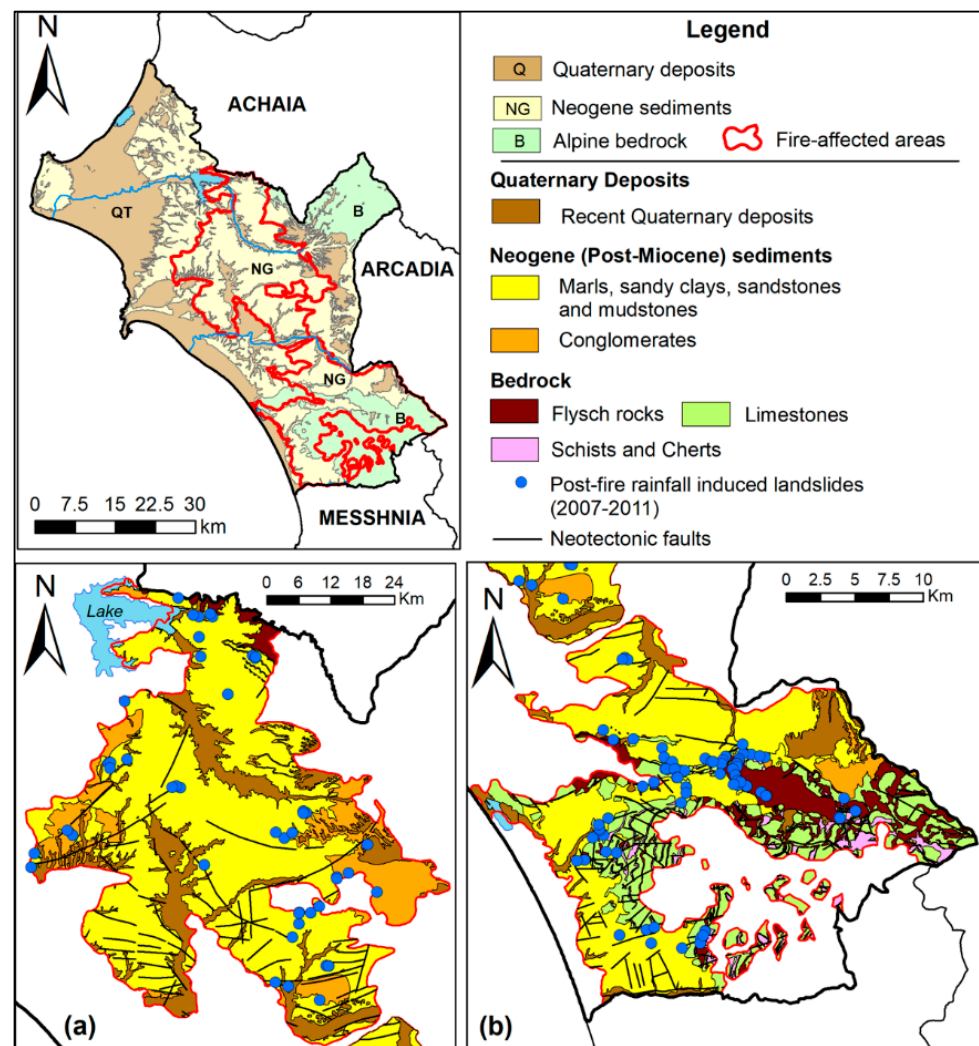


**Figure 2.** Geological map of the Ilia Regional unit with an emphasis given on the (a) North and (b) South sections (zones) of the burned areas and the post-fire rainfall-induced landslides. (From Lainas et al. [56], modified and updated).

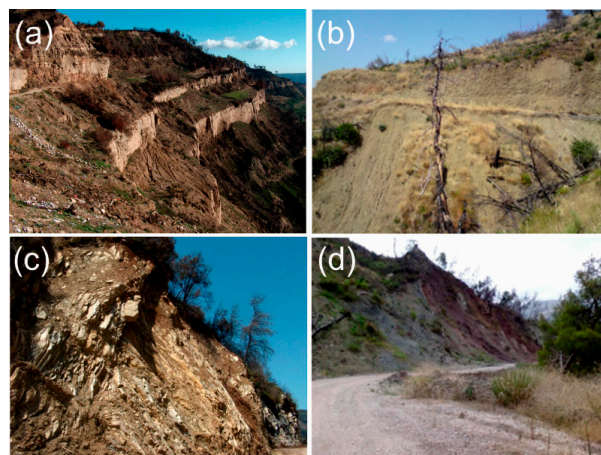


**Figure 3.** Typical geological formations in the study area. (a) Sedimentary sequences of post-Miocene sediments, showing alternating beds of sandstone and silt/mudstones, (b) typical Flysch-rock sequence with shales and mudstones underlain sandstones, (c) highly jointed limestone bedrock rock mass, (d) highly weathered schist/chert rocks.

Regional active tectonics and high seismicity [67,68] also have a significant role in the shaping of the area's morphology by forming successive tectonic horsts and grabens and influencing the surface drainage network.

The aforementioned rock types and mainly the “flysch” rocks and the post-Miocene sediments are, due to differential response to weathering processes and intense fracturing, the most susceptible to landslide phenomena geological formations, with heavy rainfall, regional climate patterns, and tectonics to be considered as the main controlling factor for landslide activation, not only in the wider area but also in overall Greece [69–74].

### 2.3. Climate Setting and Rainfall Patterns

Being affected by the Mediterranean Sea, the study area has a typical Mediterranean climate. Average monthly temperatures range between 20 °C and 25 °C during the summer months and between 4 °C to 10 °C during the winter months, with at least four months above 10 °C. As it is also shown in Figures 4 and 5, annual rainfall in the affected areas ranges approximately between 800 and 1400 mm with the lower values along the plain areas at the west and the higher values at the easternmost mountainous areas.

The rainfall patterns of the study area were examined by historical rainfall data collected through a network of ten selected meteorological gauging stations with consistent daily rainfall data, covering the period between 1977 and 2019, installed by the Ministry of Environment and Climate Change and the National Observatory of Athens. Every meteorological station along the respective Thiessen polygons that influence the neighboring landslides is also shown (Figure 4).

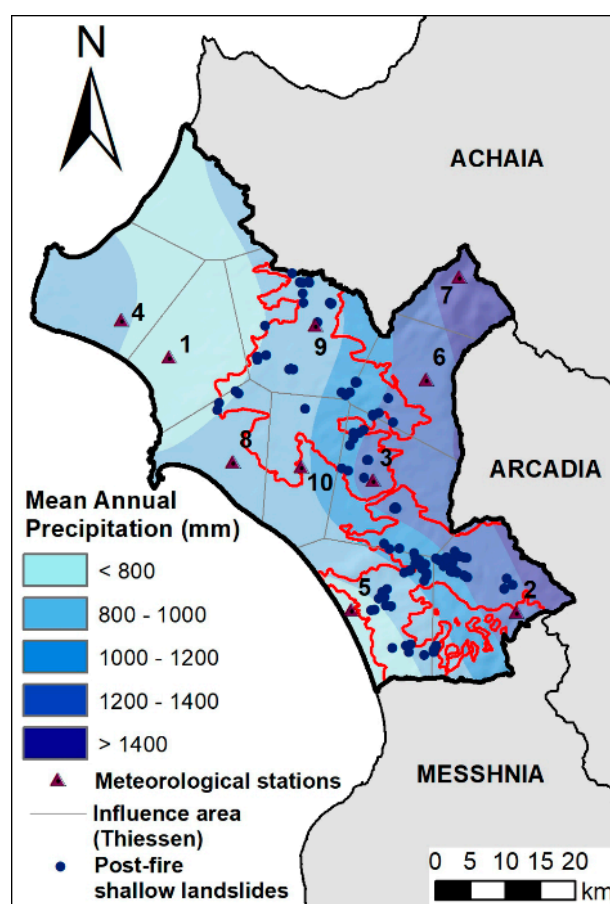
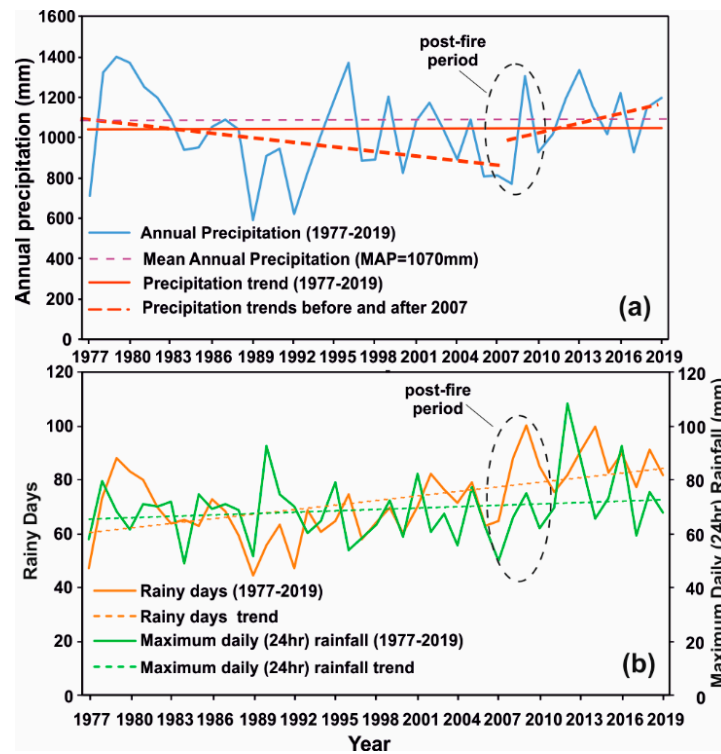


Figure 4. Mean annual rainfall map of the Ilia Regional unit during the 1977–2019 period.



**Figure 5.** Rainfall patterns of the study area during 1977–2019. (a) Annual precipitation and precipitation trends. Mean Annual Precipitation is also shown. (b) Rainy days and Maximum Daily (24 h) rainfall with corresponding trends.

Long-term variation of mean annual rainfall during the 1977–2019 period shows that the study area is characterized by dry periods 2 to 5 years long, alternating with rainy periods which last between 2 and 3 years. Mean Annual Precipitation (MAP) in the burned areas is approximately 1070 mm. Even though the general annual rainfall trend looks steady during the whole above time frame, it seems to be a change in the rainfall trend before and after 2007. A general trend of decreasing annual rainfall up to 2007 is followed by an increasing trend after 2007 (Figure 5a). Rainy days and maximum daily (24 h) rainfall seem to have increased trends for the whole period (Figure 5b).

Closer observation of seasonal rainfall variation (Figure 6) between September 2007 and May 2011 allowed to distinguish specific time frames with notable differences in regional rainfall pattern. A relatively dry period, which started before 2007 and lasted up to the end of autumn of 2008, was followed by a significantly wet first quarter of 2009 and then by a moderate to dry period until the end of 2009, with the exception of a notable rainy October of 2009. During the next nine months and until the end of 2010, rainfall values were close to corresponding averages, with the exception of an excessively rainy October. Finally, up to May 2011, monthly rainfall values were close to averages, without records of exceptional values.

The spatial and temporal variation of rainfall-induced landslides follows the aforementioned seasonal rainfall patterns. The first landslides occurred in the immediate wet season after the wildfires (Autumn 2007) and were spread throughout the affected areas as an immediate response to the effect of fires (Figure 6). During this period, monthly rainfall was close to historical averages. After this initial response and during the rest 3.5-year post-wildfire period, shallow rainfall-induced landslides were more frequent when monthly rainfall exceeded the corresponding averages and, in most, had a smaller spatial extent.

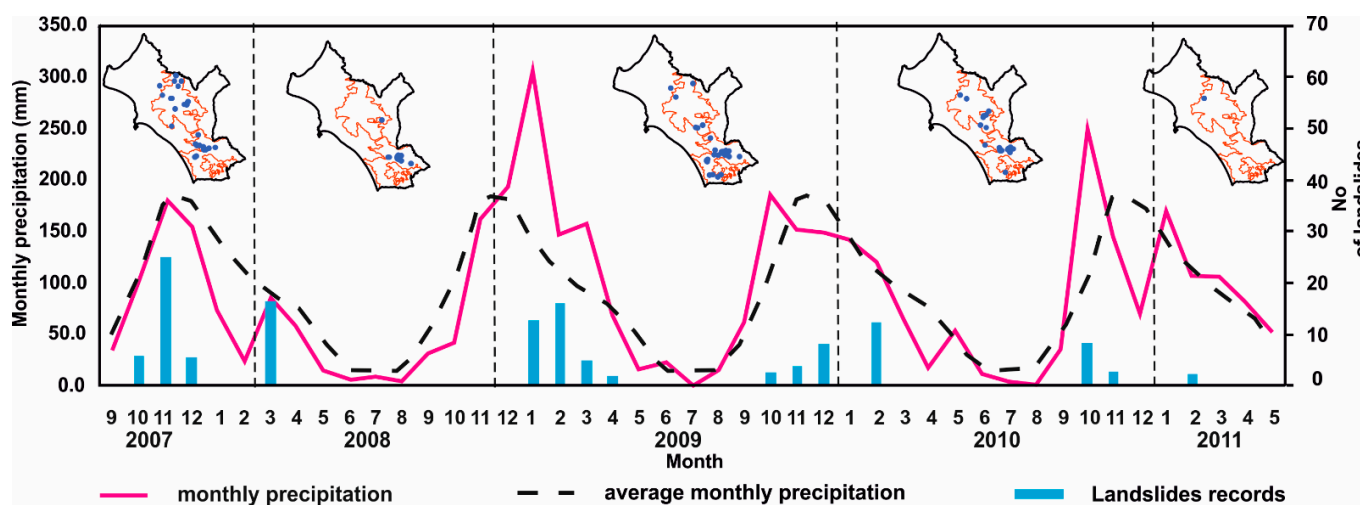


**Figure 6.** Monthly rainfall variations between September 2007 and May 2011 to monthly average values. Spatial and temporal variation of rainfall-induced landslides during post-wildfire seasons is also shown (in bars).

#### 2.4. Landslide Dataset

Landslides and soil erosion phenomena induced by rainfall affected the burned areas, particularly road networks and inhabited areas. Local authorities focused their attention on mitigating the problem by implementing small-scale remedial measures. To aid this planning, a systematic, detailed engineering geological survey was carried out [41,42,56–58] throughout the 4-year post-wildfire period (up to May 2011), including: (a) field surveys to identify and map the occurred instability phenomena, (b) detailed engineering geological and geotechnical investigations in selected landslide zones and (c) landslide recording by applying an appropriately designed Landslide Inventory Form [57,71].

A total number of 122 well defined and documented rainfall-induced landslides were recorded within the wildfire-affected areas, which were activated at least once during the period from September 2007 up to May 2011. The spatial distribution of the recorded landslide occurrences is expressed by the landslide inventory map in Figure 1. As shown in Figure 7, most landslides (56%) were recorded within the Post-Miocene (Neogene) sediments, with most of them (82%) occurring in fine-grained and mixed facies that represent 46% of the total recorded cases. In the bedrock (44%), the majority was recorded within the weathered flysch and cherts (83%), which represent 37% of the total recorded cases (Figure 7a). As shown in Figure 7b, the main type of movement, according to the classification given by Cruden and Varnes [75], is rotational sliding (81%), with a smaller number occurring as translational and composite slides, earth flows, and falls. In respect of landslide magnitude (Figure 7c), according to the classification given by Fell [76], most recorded cases represent very small landslides (72%). Typical examples of rainfall-induced landslide types in the burned areas are shown in Figure 8.

In conclusion, a landslide analysis of the burned areas showed that most of the rainfall-induced landslides were of extremely small (less than 500 m<sup>3</sup>) to small (500 < V < 1500 m<sup>3</sup>) volume [76]. Most of the landslides were shallow rotational slides and earth flows located mainly on the weathered mantle of the Neogene sediments or alpine bedrock. Phenomena of a different type, such as rockfalls, were few and were recorded only on the steepest slopes of limestones and well-cemented conglomerates.

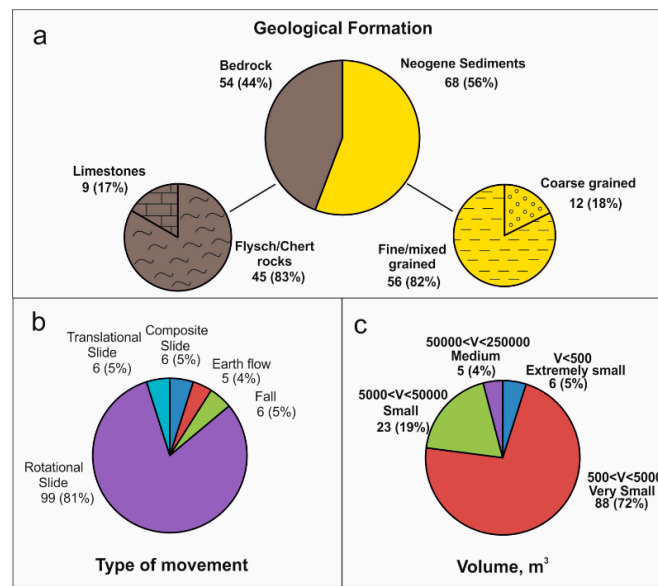


**Figure 7.** Main Characteristics of rainfall-induced landslides during the post-wildfire seasons. (a) Geological formation, (b) type of movement, (c) Volume.



**Figure 8.** Landslide phenomena in the wildfire-affected areas. (a) rotational slide in post-Miocene fine-grained sediments, (b) rotational slide in loose conglomerates and sandstones, (c) rotational slide in weathered cherts, (d) rotational slide in weathered flysch, (e) rockfall in limestones, (f) falls in cemented conglomerates, (g) earth flow in weathered flysch, (h) translational slide along normal fault plane in sandstones, (i) composite slide in post-Miocene sediments.

### 2.5. Rainfall Events and Threshold Value

For every landslide occurrence, daily rainfall data were obtained from the nearest meteorological station. The selection of the most appropriate meteorological station for each landslide was based on its proximity to the landslide location, its similarity in elevation with the landslide, the local morphological setting, and the reliability of the station records. Priority was given to meteorological stations that were located within the same watershed and had elevations close to the elevation of the respective landslide.

Having as a reference the number of days that each landslide had been activated and based on the preliminary assumption that a landslide is activated towards the last days of a rainfall event, the detailed analysis of the daily rainfall data allowed the identification of distinct rainfall events causing landslides with defined duration and a cumulative amount of rainfall.

The recorded landslides were associated with the cumulative rainfall event ( $E$ ) in respect of a certain rainfall duration ( $D$ ) that was responsible for landslide activation by using the Cumulative Event-Duration ( $ED$ ) empirical threshold equation proposed by Lainas et al. [56].

$$E = 10.95 \times D^{0.423} \quad (1)$$

when  $48 < D < 312$  h and where  $E$  is the cumulative (total) event rainfall (in mm), and  $D$  is the duration of the rainfall event (in hours).

By using the threshold equation, the corresponding rainfall values have been calculated for every duration class. Each calculated rainfall value was then used to estimate the annual landslide probability for every duration class when the corresponding threshold was exceeded. In this way, and after statistical analysis of the rainfall data, the frequency of these threshold values can be determined and used as a basis for estimating landslide probability [22]. However, it is important to recognize that the occurrence of a rainfall event that exceeds the assigned threshold value may not necessarily lead to slope failure. Some events may be redundant or even ineffective, depending on the status of the slope development and the local landslide history.

### 2.6. Exceedance Statistics and Probability

The probability of occurrence of a rainfall-induced landslide can be expressed as the product of the annual probability of the trigger (i.e., the rainfall threshold) and the conditional probability of the slope failure. The conditional probability is defined as the probability of slope failure once the rainfall threshold has been exceeded. If  $P(A)$  is the annual probability of the rainfall event exceedance and  $P(B)$  is the probability of landslide activation, the landslide probability  $P[A \cap B]$  is expressed as shown below [24]:

$$P[A \cap B] = P(A) \times P[BA] \quad (2)$$

This equation states the probability of occurrence of both events  $A$  and  $B$  (intersection probability) and is equal to the probability of occurrence of event  $A$  multiplied by the probability of occurrence of event  $B$  in the condition that event  $A$  has already occurred (conditional probability).  $P(A)$  is determined based on the assumption that

$$P(A) = P[E > E_{th}] \quad (3)$$

where  $P[E > E_{th}]$  is the annual probability of the rainfall threshold ( $E_{th}$ ) exceedance, with  $E_{th}$  corresponding to the calculated threshold for each rainfall duration class, according to Equation (1).

For the calculation of the threshold annual exceedance probability  $P(A)$  for each duration class, all rainfall events for every duration class and every meteorological station were first identified, covering all the 1977–2019 period. For example, in the case of a six-days (6) cumulative rainfall event, all events with a duration of six days were distinguished and selected through the complete series of daily rainfall. Each year's maximum value was

then selected to produce an annual exceedance series, allowing to distinguish the annual values that are higher than the corresponding calculated threshold value ( $E_{th}$ ) for each duration.

Annual exceedance probabilities ( $P(A)$ ) of each threshold value were estimated by performing separate frequency analyses at the annual exceedance series to the data of each duration class and in every meteorological station that was selected as the representative for landslide triggers. Towards this result, each annual exceedance series has been analyzed by applying the Generalized Extreme Value Distribution (EV1) function [77–79]. In order to check the fit of the data in the above probability distribution function, the Frequency Factor method was applied [79]. After plotting the annual exceedance series in a probability paper (Gumbel Plot), the linearization between the variate and the selected reduced variate is being checked. When the plot can fit with a straight line, this can be a confirmation that the checked data can fit the selected probability distribution.

In order to achieve this, the plotting positions of each annual exceedance series have been found. After sorting the annual maximums in descending order, the empirical return period was estimated, according to the Weibull formula:

$$T = \frac{N + 1}{m} \quad (4)$$

where  $N$  equals the number of years and  $m$  the position of each year in descending order.

Once the data series is ranked and the plotting positions calculated, a graph between the variate and the reduced variate is plotted to graphically fit the distribution. In the case of the Frequency Factor method, the relationship that combined the variate ( $E_T$ ) with the reduced variate ( $K_T$ ) is:

$$E_T = \mu + K_T \times \sigma \quad (5)$$

where  $\mu$  is the average,  $\sigma$  is the standard deviation of each data series. The reduced variate ( $K_T$ ) of the EV1 probability distribution function is calculated for the relationship

$$K_T = -[\bar{y}_n + \ln\{\ln(T) - \ln(T - 1)\}] / \sigma_n \quad (6)$$

where  $\bar{y}_n$  and  $\sigma_n$  represent the expected average and standard deviation parameters of the reduced variate of the Gumbel distribution and are selected from tables according to the size of the time series [77].

After calculating  $K_T$  assuming a GEV probability distribution, the  $P(A)$  for each duration class was estimated. The determination of  $P[B | A]$  relied on landslide frequency after rainfall exceeded the given threshold value for every duration class and the corresponding landslide set.

### 3. Results

The definition of each rainfall event, as it was previously mentioned, and the connection of landslides with specific rainfall events resulted in the identification of specific time windows (in days) of rainfall in the calculation of the cumulative rainfall ( $E$ ) for each event and the identification of the recorded maximum daily (R24 h) rainfall during each event. The classes of the rainfall duration ( $D$ ), along with the corresponding range of the cumulative rainfall ( $E$  in mm) and the corresponding maximum 24 h rainfall (R24 h) for each duration class were established and are shown in Table 1. It can be initially observed that rainfall events that have triggered landslides in the affected areas had a duration between 2 and 13 days, were characterized by cumulative rainfall between 56.5 and 251.5 mm, and maximum daily (24 h) rainfall within the range from 22.6 to 71.4 mm. More specifically, it can be seen that most landslides were triggered after rainfall duration in the range between 6 and 7 days and with cumulative rainfall between 95.6 to 214.4 mm.

**Table 1.** Number and rainfall patterns (Duration, cumulative rainfall, and maximum 24 h rainfall) of the rainfall events that triggered landslides in the wildfire-affected areas.

No of Rainfall Events Causing Landslides	No of Recorded Landslides	Meteorological Station (No)	Rainfall Duration (Days)	Cumulative Rainfall (E) (mm Range)	Max R24 h (mm Range)		
2	2	3,9	2	56.5	106.6	31.6	57.2
2	7	1,3,8,9	3	67.2	112.8	25.4	58.2
4	8	2,5,9	4	75.6	133.4	27.4	58.6
3	8	2,5,9	5	85.2	134.6	23.8	62.4
3	22	2	6	145.6	188.2	62.4	71.4
8	36	2,3,5,9	7	95.7	214.4	22.6	57.2
1	6	2	8	119	119	25.4	25.4
2	13	2,3,5,9	9	109	232.1	30	62.4
2	4	2,3	10	202.8	251.5	41.8	57.2
3	8	2,6,9	11	132.3	164.8	23.2	49.2
1	8	5	13	129.4	112.8	40.4	40.4

Figure 9a shows the spatial distribution of the 122 recorded landslides, which were triggered during a total of 31 rainfall events. It can be seen that most landslides were triggered after at least 6 days of cumulative rainfall, especially at the Southern zone of the burned areas, which is mainly dominated by weathered bedrock, such as flysch and cherts. Similarly, as shown in Figure 9b,c, landslides in the Southern zone are characterized by higher cumulative rainfall and higher maximum daily rainfall (R24 h) values.

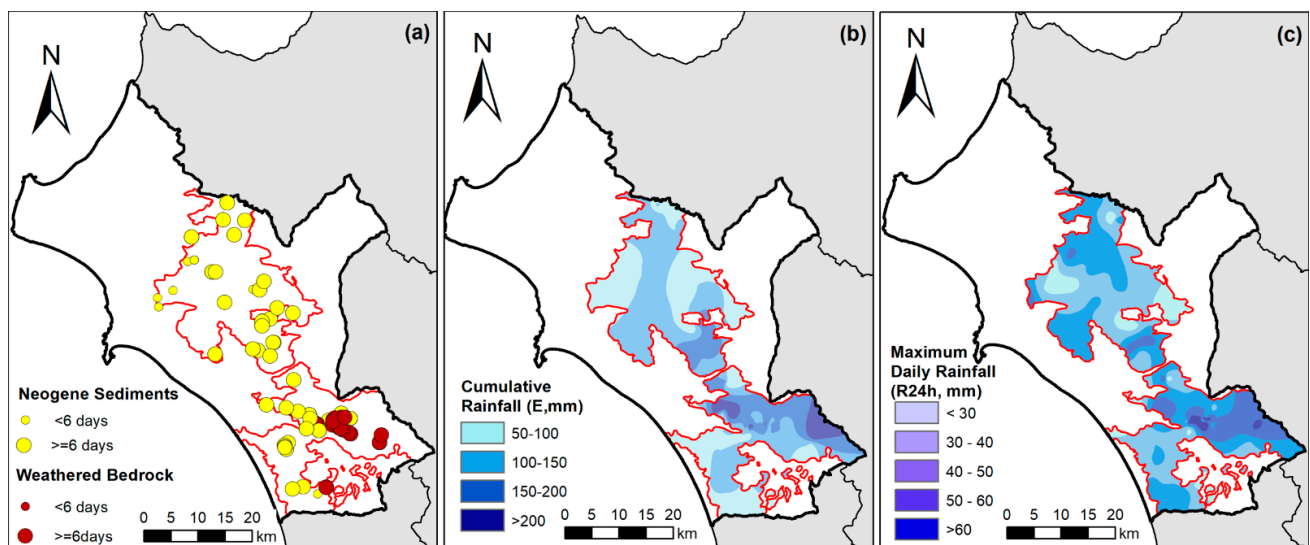


**Figure 9.** Spatial distribution of (a) rainfall duration, (b) cumulative rainfall, and (c) maximum daily rainfall of the landslide-trigger rainfall events during the post-wildfire period.

In more detail and as shown in Table 2, approximately 85% of the landslides of the South zone of the burned areas required cumulative rainfall of at least 6 days for their activation. On the contrary, in the North zone, this percentage was lower (about 67%). In addition, landslide triggering in the North zone required less than 200 mm of cumulative rainfall, whereas, in the South, 13.4% of the landslides required more than 200 mm of cumulative rainfall to be activated. Similarly, the recorded maximum daily rainfall was for all landslides of the North zone lower than 60 mm, whereas for the South, this value was not adequate for the 29% of the recorded cases.

**Table 2.** Lithology and rainfall parameters (Duration, Cumulative Rainfall, and Maximum Daily (24 h) Rainfall) of the recorded landslides at the North and South Zone of the burned areas.

Category		Landslides North Zone (No (%))	Landslides South Zone (No (%))
Lithology	Neogene sediments	39 (100%)	29 (34.9%)
	Weathered bedrock	0 (0%)	54 (65.1%)
Duration (D, days)	<6	13 (33.3%)	26 (14.5%)
	≥6	12 (66.7%)	71 (85.5%)
Cumulative Rainfall (E, mm)	50–<100	13 (33.3%)	22 (26.5%)
	100–<150	17 (43.6%)	28 (33.7%)
	150–<200	9 (23.1%)	22 (26.5%)
	≥200	0 (0%)	11 (13.3%)
Maximum Daily Rainfall (R24 h, mm)	<30	6 (15.4%)	8 (9.6%)
	30–<40	10 (25.6%)	7 (8.4%)
	40–<50	14 (35.9%)	33 (39.8%)
	50–<60	9 (23.1%)	11 (13.3%)
	≥60	0 (0%)	24 (28.9%)

Plotting of the Cumulative rainfall (E) and rainfall Duration (D) of the recorded landslide cases during the post-wildfire period in respect of the rainfall data (E-D diagram) is shown in Figure 10, together with the corresponding rainfall threshold. In Figure 10 it can also be observed that the majority of rainfall-induced recorded landslides were triggered after 144 h (6 days) of cumulative rainfall and, more precisely, between 6 and 7 days.

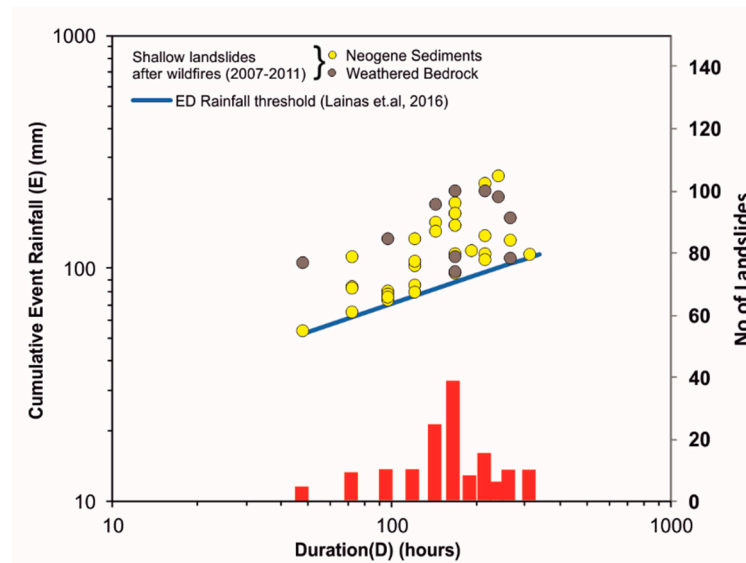


**Figure 10.** Rainfall threshold for possible shallow landslide trigger in wildfire affected areas [56]. Post-fire landslides are shown in both Neogene and weathered bedrock, as well as the landslide distribution in respect to duration.

The application of the threshold equation for each duration class, as it was previously analysed, and the rainfall data frequency analysis resulted in the calculated probabilities of Table 3. In the cases when data from more than one meteorological station was analyzed for each rainfall duration class, average values of  $P(A)$  are shown in Table 3. As an example, a rainfall event with a duration of 6 days corresponds to a rainfall threshold value of 95.66 mm. After statistical analysis of daily rainfall, such a rainfall event has an annual exceedance probability  $P(A)$  equal to 0.964. The conditional probability ( $P[B|A]$ ) can be calculated for this case as  $36/122 = 0.295$  and the final probability  $P[A \cap B] = 0.284$

(approximately 1 every 3). In terms of the return period, this annual probability can also be expressed as  $T = 1/0.284 = 3.52$  years.

**Table 3.** Annual probability calculations and classification of shallow rainfall-induced landslides related to the Rainfall threshold (ED) and the rainfall duration class (D).

D (Days)	ED (mm)	No of Landslides	P(A)	P(B   A)	P(A ∩ B)	Probability Classification
2	56.31	2	0.763	0.016	0.012	Medium
3	66.84	7	0.705	0.057	0.040	Medium–High
4	75.49	8	0.864	0.067	0.058	High
5	82.97	8	0.709	0.067	0.048	High
6	89.62	22	0.999	0.180	0.180	High
7	95.66	36	0.964	0.295	0.284	High–Very High
8	101.22	6	0.990	0.049	0.049	High
9	106.39	13	0.776	0.107	0.083	High
10	111.24	4	0.973	0.033	0.032	Medium
11	115.81	8	0.719	0.066	0.047	Medium–High
13	124.29	8	0.552	0.066	0.036	Medium

Figure 11 shows the classification of annual probability according to Fell [76]. It can be concluded that shallow landslide response in wildfire-affected areas has a higher annual probability for rainfall events with a total duration between 6 and 9 days. In these cases, both the return period of the corresponding rainfall event is low, and the landslide frequency is high, resulting in high to very high annual probabilities. For a duration of less than six (6) days, estimated annual probabilities were found to be lower. The return period of rainfall events for this duration range is higher than longer durations, and, at the same time, landslide frequency is lower. This means that intense rainfall events of small duration did not have a primary impact in the affected areas, but between duration and cumulative rainfall, the total rainfall volume was more important in the activation of landslides.

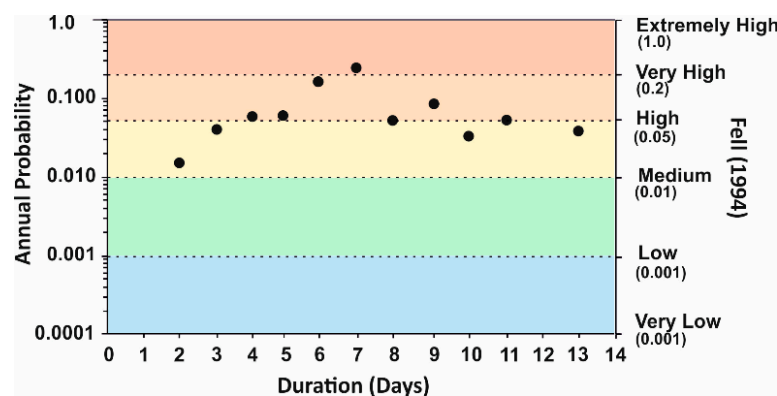


**Figure 11.** Annual Probability calculations in every duration class for shallow landslide trigger in the study area.

On the other hand, landslides, which were triggered after cumulative rainfall of a duration of more than nine (9) days, also have medium to high annual probabilities. The return period of rainfall events for this duration range is in most cases among the lower, but at the same time, landslide records are also not so frequent. These cases usually represent less frequent larger and deeper rotational landslides, the activation of which is associated not only with a specific rainfall event but also with seasonal antecedent rainfall.

The spatial extent of annual landslide probability classes is also given in the landslide hazard map of Figure 12. It can be observed that higher annual probabilities for landslide triggers are observed in the central and easternmost parts of the affected areas. Both

mentioned areas have similarities and differences in respect to the conditions that may favor landslide activation. The central part is mostly dominated by fine-grained Neogene sediments, the easternmost regions mainly by weathered bedrock with both geological formations to be recognized as the most susceptible to landsliding in the study area. On the other hand, the central part is characterized by higher human impact in terms of urban development and land use but lower rainfall, while the eastern is characterized by higher altitudes, steep terrain, higher rainfall but less human impact.

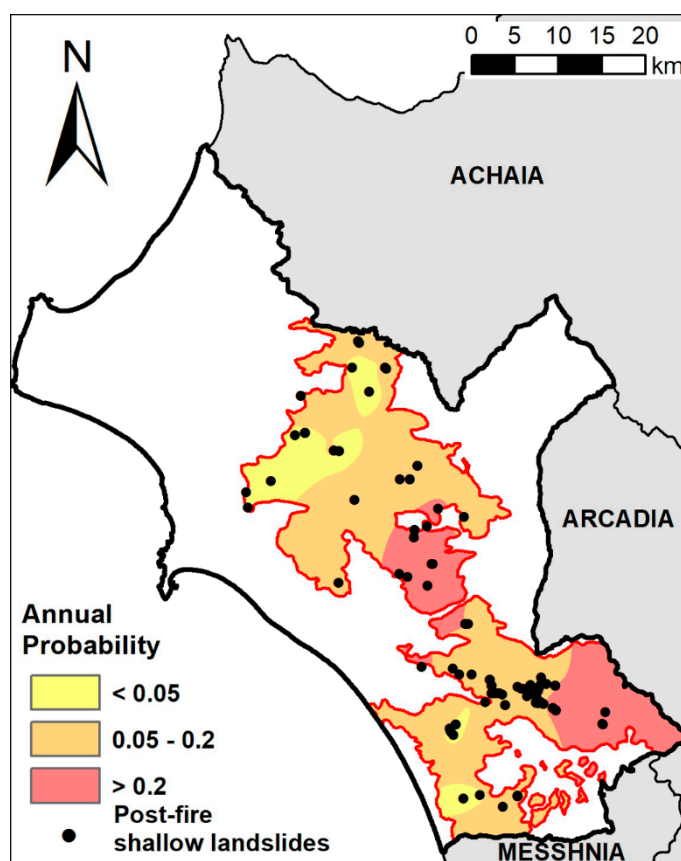


**Figure 12.** Landslide hazard zonation map showing the annual Probability for shallow landslide trigger in the study area.

#### 4. Discussion

This study presents a methodology for landslide forecasting by applying an empirical rainfall threshold model. It aims to contribute to the clarification of the role of rainfall in the activation of shallow landslides which have been triggered by heavy rainfall in either natural or excavated slopes within areas that have been previously affected by wildfires. The use of such a model is appropriate for shallow landslide monitoring in areas that pose a high susceptibility to landslides, either due to predisposing causal factors or extreme conditions of a triggering factor, such as rainfall, often combined with other environmental factors, as for example vegetation loss by forest fires.

The landslide dataset included 122 well-defined and documented, rainfall-induced landslide occurrences, which were recorded within the fire-affected areas and had been activated at least once in a period 3.5 years after the wildfires. Most of the recorded landslides were recorded within fine-grained and mixed Neogene sediments, as well as in the upper highly weathered layers of flysch and cherts. The biggest percentage of these landslides were classified as shallow and surficial rotational slides with lesser translational slides, composite slides, earth flows, and rock falls. According to Fell's classification [76],

most of the recorded cases represent very small landslides with a total volume between 500 and 5000 m<sup>3</sup>.

The North zone of the burned studied area is mostly covered by Neogene sediments, while the South is dominated by weathered bedrock with a smaller percentage of Neogene sediments. Analysis of the rainfall triggering parameters in both zones showed that landslides of the South zone required longer as well as heavier rainfall, both in terms of cumulative and maximum daily rainfall to get triggered. Furthermore, apart from their inherent lithological differences and the different rainfall patterns, which favored landslide activation in the two burned zones, their differences in the land cover before the fires as well as the different degree of human impact had also influenced landslide activity.

The estimation of the annual exceedance probability of the ED rainfall threshold for each duration class showed that shallow landslide response in the study area has higher annual probabilities for rainfall events with a total duration between six (6) and nine (9) days. For the duration range shorter than six (6) days, estimated annual probabilities were found to be lower. Individual and intense rainfall events of small duration were not adequate to activate landslides but the required amount of rainfall for slope failures was higher.

On the other hand, landslides that were triggered after cumulative rainfall of duration more than nine (9) days also have medium to high annual probabilities. The return period of rainfall events for this duration range is in most cases among the lower, but at the same time, landslide records are not so frequent. In this case, as well as in longer rainfall durations, the application of a simple threshold methodology can be questionable and should be used with appropriate judgment. Besides, the nature of a recently burned area in terms of short-term response in rainfall typically favors the manifestation of shallow or even surficial landslide phenomena. Deeper landslides in a recently burned area can also start with a small rate of movement and gradually develop in larger landslides, under the influence of seasonal antecedent rainfall and taking into consideration the regeneration of the burned vegetation. Modelling of these cases is preferably being done at a larger scale by applying site-specific geotechnical models with local rainfall thresholds, including soil parameters connected with the status and level of root reinforcement before and after the fires [24,80].

The proposed methodology for shallow landslide forecasting in wildfire-affected areas focus on the quantification of the main triggering factor, which in our case is heavy rainfall. In detail, the result of the proposed methodology is to provide probability estimates for landslide occurrence over burned areas after a severe rainfall event and before the construction of remedial works. In the study area, several landslide remedial works were implemented by the regional authorities during and after the post-wildfire period, focusing on protecting infrastructures and settlements. Remedial measures mainly consisted of traditional engineering techniques, including typical drainage control works, slope reshaping, road repairing, and typical stabilization structures, such as gabion structures or concrete retaining walls. Most of them were considered as small-scale constructions works of fast application, aiming to either repair the damages or to control water runoff. All remedial works were constructed according to local knowledge, availability of resources, and materials.

It is expected that in most cases, the applied remedial works reduced the probability of landsliding. However, the effectiveness of remedial measures in stabilizing recently burned slopes is under research by the authors in specific landslide cases by using 2D or 3D geotechnical models. In this context, it would be interesting to incorporate into the geotechnical model the effect of vegetation regeneration in topsoil properties as well as the reinforcement provided by root reinforcement under the influence of heavy rainfall. The application of soil-bioengineering techniques [81–84] presents an innovative method for slope stabilization, which is also more compatible with the natural environment and usually with smaller implementation and maintenance costs. Comparative analyses of the effectiveness between traditional engineering works and soil bioengineering techniques

can reach useful conclusions and provide guidelines towards the most effective way for the remediation of burned slopes; thus, minimizing the danger of shallow slope failures during the post-fire period.

## 5. Conclusions

This study presents a proposed empirical rainfall threshold for the possible shallow landslide occurrence in burned areas to estimate annual probabilities for shallow landslide activation. It aims to contribute to the development of a novel methodology for shallow landslide forecasting and monitoring in areas that have suffered significant natural disasters, such as forest fires. Furthermore, it presents the relationship existing between landslide response and rainfall, and how this is affected by the land use patterns, geological conditions, and degree of human impact. However, the proposed methodology, as a simple predictive model, must consider some inherent drawbacks. Even though the exceedance of a certain rainfall threshold is necessary to landslide activation, it is not the only sufficient factor that contributes to trigger a mass movement. Studying an area that has suffered a significant natural disaster and under specific geological and climatic conditions, which are among the main factors that contribute to landslide movement, represents a useful example in the context of rainfall-induced landslide research.

Another specific objective of this research is to present the role of rainfall in landslide hazard, especially within the concept of Climate Change. According to the Climate projection scenarios for the 21st century, the mean annual precipitation in many areas, including Southern Europe, is projected to remain constant, but concentrated in a fewer number of rainy days, resulting in more intense rainfall events, anticipating more frequent shallow landslides [60].

Another outcome of this research is to provide an estimation of the annual probability occurrence of shallow rainfall-induced landslides in relation to the Rainfall threshold (ED), which can be applied to landslide forecasting before any remedial works are carried out. The proposed methodology for this type of estimation is sensitive to the details of the landslide dataset and the nature of the study area and can be greatly affected by any remedial works. The effect of the remedial works represents a task of further research, which is in progress by the authors in specific landslide areas by applying local geotechnical landslide activation models under the influence of heavy rainfall.

In conclusion this study provides preliminary results at a regional scale and is a first step for the implementation of a landslide forecasting tool in an applied form. Towards this goal, the quantification of the rainfall patterns that act as trigger mechanisms on landslides in a specific area is of great importance when analysis of selected landslide cases is required.

**Author Contributions:** Conceptualization, S.L.; methodology, S.L.; validation, S.L., N.D. and N.S.; formal analysis, S.L.; investigation, S.L, N.D. and N.S.; resources, S.L., N.D. and N.S.; data curation, S.L. and N.D.; writing—original draft preparation, S.L.; writing—review and editing, S.L. and N.D.; visualization, S.L. and N.D.; supervision, N.D. and N.S.; project administration, N.S.; funding acquisition, N.D. All authors have read and agreed to the published version of the manuscript.

**Funding:** This publication has been financed by the Research Committee of the University of Patras. The respective fieldwork research has been financed by the Region of Western Greece.

**Data Availability Statement:** Landslide data of this research can be found in <http://landslide.engeolab.gr/>, which hosts a Multi Administration Information System of Landslides in Western Greece designed by the Laboratory of Engineering Geology of University of Patras.

**Acknowledgments:** The authors are grateful to all the anonymous residents of the wildfire-affected areas, as well as the local authorities, for their overall help and contribution during the extensive field visits in the affected areas.

**Conflicts of Interest:** The authors declare no conflict of interest. The funders had no role in the design of the study, in the collection, analyses, or interpretation of data, in the writing of the manuscript, or in the decision to publish the results.

## References

1. Caine, N. The rainfall intensity-duration control of shallow landslides and debris flows. *Geogr. Ann.* **1980**, *62A*, 23–27.
2. Guzzetti, F.; Peruccacci, S.; Rossi, M.; Stark, C.P. Rainfall thresholds for the initiation of landslides in central and southern Europe. *Meteorol. Atmos. Phys.* **2007**, *98*, 239–267. [[CrossRef](#)]
3. Guidicini, G.; Iwasa, O.Y. Tentative correlation between rainfall and landslides in the humid tropical environment. *Bull. Int. Assoc. Eng. Geol.* **1977**, *16*, 13–20. [[CrossRef](#)]
4. Fukuoka, M. Landslides associated with rainfall. *Geotech. Eng.* **1980**, *11*, 1–29.
5. Canuti, P.; Focardi, P.; Garzonio, C.A. Correlation between rainfall and landslides. *Bull. Int. Assoc. Eng. Geol.* **1985**, *32*, 49–54. [[CrossRef](#)]
6. Cannon, S.H. Regional rainfall-threshold conditions for abundant debris-flow activity. In *Landslides, Floods, and Marine Effects of the Storm of 3–5 January 1982, in the San Francisco Bay Region California*; Ellen, S.D., Wieczorek, G.F., Eds.; US Government Printing Office: Boston, MA, USA, 1982; Volume 1434, pp. 35–42.
7. Montgomery, D.R.; Dietrich, W.E. A physically based model for the topographic control of shallow landsliding. *Water Resour. Res.* **1994**, *30*, 1153–1171. [[CrossRef](#)]
8. Ayalew, L. The effect of seasonal rainfall on landslides in the highlands of Ethiopia. *Bull. Int. Assoc. Eng. Geol.* **1999**, *58*, 9–19. [[CrossRef](#)]
9. Corominas, J.; Moya, J. Reconstructing recent landslide activity in relation to rainfall in the Llobregat River basin, Eastern Pyrenees, Spain. *Geomorphology* **1999**, *30*, 79–93. [[CrossRef](#)]
10. Calcaterra, D.; Parise, M.; Palma, B.; Pelella, L. The influence of meteoric events in triggering shallow landslides in pyroclastic deposits of Campania, Italy. Landslides in Research, Theory and Practice. In Proceedings of the 8th International Symposium on Landslides, Cardiff, UK, 26–30 June 2000; Volume 1, pp. 209–214.
11. Iverson, R.M. Landslide triggering by rain infiltration. *Water Resour. Res.* **2000**, *36*, 1897–1910. [[CrossRef](#)]
12. Ahrendt, A.; Zuquette, L.V. Triggering factors of landslides in Campos do Jordao city, Brazil. *Bull. Int. Assoc. Eng. Geol.* **2000**, *62*, 231–244. [[CrossRef](#)]
13. Ibsen, M.L.; Casagli, N. Rainfall patterns and related landslide incidence in the Porretta-Vergato region, Italy. *Landslides* **2004**, *1*, 143–150. [[CrossRef](#)]
14. Crosta, G.B.; Frattini, P. Rainfall thresholds for triggering soil slips and debris flow. In Proceedings of the 2nd EGS Plinius Conference on Mediterranean Storms, Siena, Italy, 1–3 October 2001; pp. 463–487.
15. Godt, J.W. Observed and Modeled Conditions for Shallow Landsliding in the Seattle, Washington Area. Ph.D. Thesis, University of Colorado, Fort Collins, CO, USA, 2004.
16. Giannecchini, R. Rainfall triggering soil slips in the southern Apuane Alps (Tuscany, Italy). *Adv. Geosci.* **2005**, *2*, 21–24. [[CrossRef](#)]
17. Wieczorek, G.F.; Glade, T. Climatic factors influencing occurrence of debris flows. In *Debris Flow Hazards and Related Phenomena*; Jakob, M., Hungr, O., Eds.; Springer: Berlin/Heidelberg, Germany, 2005; pp. 325–362.
18. Cardinali, M.; Galli, M.; Guzzetti, F.; Ardizzone, F.; Reichenbach, P.; Bartoccini, P. Rainfall induced landslides in December 2004 in south-western Umbria, central Italy: Types, extent, damage and risk assessment. *Nat. Hazards Earth Syst. Sci.* **2006**, *6*, 237–260. [[CrossRef](#)]
19. Salciarini, D.; Godt, J.W.; Savage, W.Z.; Conversini, P.; Baum, R.L.; Michael, J.A. Modeling regional initiation of rainfall-induced shallow landslides in the eastern Umbria Region of central Italy. *Landslides* **2006**, *3*, 181–194. [[CrossRef](#)]
20. Gabet, E.J.; Burbank, D.W.; Putkonen, J.K.; Pratt-Sitaul, B.A.; Ojha, T. Rainfall thresholds for landsliding in the Himalayas of Nepal. *Geomorphology* **2004**, *63*, 131–143. [[CrossRef](#)]
21. Zezere, J.L.; Trigo, R.M.; Trigo, I.F. Shallow and deep landslides induced by rainfall in the Lisbon region (Portugal): Assessment of relationships with the North Atlantic Oscillation. *Nat. Hazards Earth Syst. Sci.* **2005**, *5*, 331–344. [[CrossRef](#)]
22. Chleborad, A.F.; Baum, R.L.; Godt, J.W. *Rainfall Thresholds for Forecasting Landslides in the Seattle, Washington, Area-Exceedance and Probability*; US Geological Survey Open-File Report; US Geological Survey: Reston, VA, USA, 2006; Volume 1064, pp. 1–31.
23. Guzzetti, F.; Peruccacci, S.; Rossi, M.; Stark, C.P. The rainfall intensity-duration control of shallow landslides and debris flows: An update. *Landslides* **2008**, *5*, 3–17. [[CrossRef](#)]
24. Floris, M.; Bozzano, F. Evaluation of landslide reactivation: A modified rainfall threshold model based on historical records of rainfall and landslides. *Geomorphology* **2008**, *94*, 40–57. [[CrossRef](#)]
25. Dahal, R.K.; Hasegawa, S. Representative rainfall thresholds for landslides in Nepal Himalaya. *Geomorphology* **2008**, *100*, 429–443. [[CrossRef](#)]
26. Brunetti, M.T.; Peruccacci, S.; Rossi, M.; Luciani, S.; Valigi, D.; Guzzetti, F. Rainfall thresholds for the possible occurrence of landslides in Italy. *Nat. Hazards Earth Syst. Sci.* **2010**, *10*, 447–458. [[CrossRef](#)]
27. Peruccacci, S.; Brunetti, M.T.; Luciani, S.; Vennari, C.; Guzzetti, F. Lithological and seasonal control on rainfall thresholds for the possible initiation of landslides in central Italy. *Geomorphology* **2012**, *139*, 79–90. [[CrossRef](#)]
28. Segoni, S.; Piciullo, L.; Gariano, S.L. A review of the recent literature on rainfall thresholds for landslide occurrence. *Landslides* **2018**, *15*, 1483–1501. [[CrossRef](#)]
29. Fusco, F.; De Vita, P.; Mirus, B.B.; Baum, R.L.; Allocca, V.; Tufano, R.; Clemente, E.D.; Calcaterra, D. Physically based estimation of rainfall thresholds triggering shallow landslides in volcanic slopes of Southern Italy. *Water* **2019**, *11*, 1915. [[CrossRef](#)]

30. Swanson, F.J. Fire and geomorphic processes. In *Fire Regimes and Ecosystem Properties*; Mooney, H.A., Bonnicksen, T.H., Christensen, N.L., Lotan, J.E., Reiners, W.A., Eds.; USDA Forest Service General Technical Report; USDA Forest Service: Washington, DC, USA, 1981; Volume WO-26, pp. 401–420.
31. Spittler, T.E. Fire and the debris flow potential of winter storms. In *Brushfires in California Wildlands: Ecology and Resource Management*; Keeley, J.E., Scott, T., Eds.; International Association of Wildland Fire: Fairfield, WA, USA, 1995; pp. 113–120.
32. Martin, D.A.; Moody, J.A. Comparison of soil infiltration rates in burned and unburned mountainous watersheds. *Hydrol. Process.* **2001**, *15*, 2893–2903. [[CrossRef](#)]
33. Meyer, G.A.; Pierce, J.L.; Wood, S.L.; Jull, A.J.T. Fire, storms and erosional events in the Idaho Batholith. *Hydrol. Process.* **2001**, *15*, 3025–3038. [[CrossRef](#)]
34. Wondzell, S.M.; King, J.G. Post-fire erosional processes in the Pacific Northwest and Rocky Mountain Regions. *For. Ecol. Manag.* **2003**, *178*, 75–87. [[CrossRef](#)]
35. Cannon, S.H.; Gartner, J.E.; Holland-Sears, A.; Thurston, B.M.; Gleason, J.A. Debris-flow response of basins burned by the 2002 Coal Seam and Missionary Ridge fires, Colorado. In *Engineering Geology in Colorado—Contributions, Trends, and Case Histories*; Boyer, D.D., Santi, P.M., Rogers, W.P., Eds.; AEG Special Publication 14; Association of Engineering Geologists: Brunswick, OH, USA, 2003; p. 31.
36. Cannon, S.H.; Gartner, J.E. Wildfire-related debris flow from a hazards perspective. In *Debris-Flow Hazards and Related Phenomena*; Jakob, M., Hungr, O., Eds.; Springer: Berlin/Heidelberg, Germany, 2005.
37. Klock, G.O.; Helvey, J.D. Debris flows following wildfire in North Central Washington. In Proceedings of the Third Federal Inter-Agency Sedimentation Conference, Denver, CO, USA, 22–25 March 1976; pp. 91–98.
38. Morton, D.M. Distribution and frequency of storm-generated soil slips on burned and unburned slopes, San Timoteo Badlands, Southern California. In *Landslides in a Semi-Arid Environment with Emphasis on the Inland Valleys of Southern California*; Sadler, P.M., Morton, D.M., Eds.; Publications of the Inland Geological Society: Riverside, CA, USA, 1989; Volume 2, pp. 279–284.
39. Cannon, S.H.; Kirkham, R.M.; Parisem, M. Wildfire-related debris-flow initiation processes, Storm King Mountain, Colorado. *Geomorphology* **2001**, *39*, 171–188. [[CrossRef](#)]
40. May, C.L.; Gresswell, R.E. Processes and rates of sediment and wood accumulation in headwater streams of the Oregon Coast Range, USA. *Earth. Surf. Process. Landf.* **2003**, *28*, 409–424. [[CrossRef](#)]
41. Koukis, G.; Sabatakakis, N.; Lainas, S.; Depountis, N.; Skias, S. Engineering geological investigation of heavy rainfall induced landslides in wildfire affected areas, western Greece. In Proceedings of the Geologically Active, 11th IAEG congress, Auckland, New Zealand, 5–10 September 2010; pp. 331–338.
42. Depountis, N.; Lainas, S.; Pyrgakis, D.; Sabatakakis, N.; Koukis, G. Engineering Geological and geotechnical investigation of landslide events in wildfire affected areas of Ilia Prefecture, Western Greece. In *Bulletin of the Geological Society of Greece, Proceedings of the 12th International Congress of the Geological Society of Greece; Patras, Greece, 19–22 May 2010*; Geological Society of Greece: Athens, Greece, 2010; Volume 3, pp. 1138–1148.
43. Rengers, F.K.; McGuire, L.A.; Oakley, N.S.; Kean, J.W.; Staley, D.M.; Tang, H. Landslides after wildfire: Initiation, magnitude, and mobility. *Landslides* **2020**, *17*, 2631–2641. [[CrossRef](#)]
44. Vergani, C.; Werlen, M.; Conedera, M.; Cohen, D.; Schwarz, M. Investigation of root reinforcement decay after a forest fire in a Scots pine (*Pinus sylvestris*) protection forest. *For. Ecol. Manag.* **2017**, *400*, 339–352. [[CrossRef](#)]
45. Gehring, E.; Conedera, M.; Maringer, J.; Giadrossich, F.; Guastini, E.; Schwarz, M. Shallow landslide disposition in burnt European beech (*Fagus sylvatica* L.) forests. *Sci. Rep.* **2019**, *9*, 8638. [[CrossRef](#)]
46. Ko Ko, C.; Flentje, P.; Chowdbury, R. Landslides qualitative hazard and risk assessment method and its reliability. *Bull. Eng. Geol. Environ.* **2004**, *63*, 149–165. [[CrossRef](#)]
47. Melillo, M.; Brunetti, M.T.; Peruccacci, S.; Gariano, S.L.; Roccati, A.; Guzzetti, F. A tool for the automatic calculation of rainfall thresholds for landslide occurrence. *Environ. Model. Softw.* **2018**, *105*, 230–243. [[CrossRef](#)]
48. Abraham, M.T.; Satyam, N.; Rosi, A.; Pradhan, B.; Segoni, S. Usage of antecedent soil moisture for improving the performance of rainfall thresholds for landslide early warning. *Catena* **2021**, *200*, 105147. [[CrossRef](#)]
49. Onodera, T.; Yoshinaka, R.; Kazama, H. Slope failures caused by heavy rainfall in Japan. In Proceedings of the 2nd International Congress of the International Association of Engineering Geology, Sao Paulo, Brazil, 18–24 August 1974; Volume 11, pp. 1–10.
50. Kim, S.K.; Hong, W.P.; Kim, Y.M. Prediction of rainfall-triggered landslides in Korea. In Proceedings of the 6th International Symposium on Landslides, Christchurch, New Zealand, 10–14 February 1991; pp. 989–994.
51. Alleoti, P. A warning system for rainfall-induced shallow failures. *Eng. Geol.* **2004**, *73*, 247–265. [[CrossRef](#)]
52. Naidu, S.; Sajinkumar, K.S.; Oommen, T.; Anuja, V.; Samuel, R.; Muraleedharan, C. Early warning system for shallow landslides using rainfall threshold and slope stability analysis. *Geosci. Front.* **2017**, *9*, 1871–1882. [[CrossRef](#)]
53. Piciullo, L.; Calvello, M.; Cepeda, J. Territorial early warning systems for rainfall-induced landslides. *Earth-Sci. Rev.* **2018**, *179*, 228–247. [[CrossRef](#)]
54. Farina, P.; Catani, F.; Rosi, A.; Setiawan, I.; Junaidi, A.; Afrizal, K.; Wijayanto, A. Development of an early warning system for shallow landslide hazard in the Grasberg area, Indonesia. In Proceedings of the Slope Stability 2020; Dight, P.M., Ed.; Australian Centre for Geomechanics: Perth, Australia, 2020; pp. 1425–1438.
55. Valenzuela, P.; Zêzere, J.L.; Domínguez-Cuesta, M.J.; Mora García, M.A. Empirical rainfall thresholds for the triggering of landslides in Asturias (NW Spain). *Landslides* **2019**, *16*, 1285–1300. [[CrossRef](#)]

56. Lainas, S.; Sabatakakis, N.; Koukis, G. Rainfall thresholds for possible landslide initiation in wildfire-affected areas of western Greece. *Bull. Eng. Geol. Environ.* **2016**, *75*, 883–896. [[CrossRef](#)]
57. Lainas, S. Landslide Hazard Estimation in Geological Formations of Northwestern Peloponnese. Ph.D. Thesis, University of Patras, Patras, Greece, 2018.
58. Dikau, R.; Schrott, L. The temporal stability and activity of landslides in Europe with respect to climatic change (TESLEC): Main objectives and results. *Geomorphology* **1999**, *30*, 1–12. [[CrossRef](#)]
59. Seneviratne, S.I.; Nicholls, N.; Easterling, D.; Goodess, C.M.; Kanae, S.; Kossin, J.; Luo, Y.; Marengo, J.; McInnes, K.; Rahimi, M.; et al. Changes in climate extremes and their impacts on the natural physical environment. In *Managing the Risks of Extreme Events and Disasters to Advance Climate Change*; Field, C.B., Barros, V., Stocker, T.F., Qin, D., Dokken, D.J., Ebi, K.L., Mastrandrea, M.D., Mach, K.J., Plattner, G.K., Allen, S.K., et al., Eds.; A Special Report of Working Groups I and II of the Intergovernmental Panel on Climate Change (IPCC); Cambridge University Press: Cambridge, UK; New York, NY, USA, 2012; pp. 109–230.
60. Gariano, S.L.; Guzzetti, F. Landslides in a changing climate. *Earth-Sci. Rev.* **2016**, *162*, 227–252. [[CrossRef](#)]
61. Guerriero, L.; Ruzza, G.; Calcaterra, D.; Di Martire, D.; Guadagno, F.M.; Revellino, P. Modelling prospective flood hazard in a changing climate, Benevento province, southern Italy. *Water* **2020**, *12*, 2405. [[CrossRef](#)]
62. Depountis, N.; Michalopoulou, M.; Kavoura, K.; Nikolakopoulos, K.; Sabatakakis, N. Estimating Soil Erosion Rate Changes in Areas Affected by Wildfires. *Int. J. Geo-Inf.* **2021**, *9*, 562. [[CrossRef](#)]
63. Depountis, N.; Vidali, M.; Kavoura, K.; Sabatakakis, N. Soil erosion prediction at the water reservoir's basin of Pineios dam, Western Greece, using the Revised Universal Soil Loss Equation (RUSLE) and GIS. *WSEAS Trans. Environ. Dev.* **2018**, *14*, 457–463.
64. Kamperis, E. Geological and Petroleum Study of NW Peloponnese, Greece. Ph.D. Thesis, School of Mining Engineering and Metallurgy, NTUA, Zografou, Greece, 1987.
65. Frydas, D. Biostratigraphische Untersuchungen aus den Neogen der NW- und W-Peloponnes. *Neues Jahrb. Geol. Paläontol.* **1989**, *6*, 321–344.
66. Bonneau, M. Correlation of the Hellenide nappes in the southeast Aegean and their tectonic reconstruction. In *The Geological Evolution of the Eastern Mediterranean*; Dixon, J.E., Robertson, A.H.F., Eds.; The Geological Society of London Special Publication: London, UK, 1984; Volume 17, pp. 517–527.
67. Mariolakos, I.; Papanikolaou, D.; Lagios, E. A neotectonic geodynamic model of peloponnesus based on morphotectonics, repeated gravity measurements and seismicity. *Geol. Jahrb. Band* **1985**, *50*, 3–17.
68. Koukouvelas, I.; Mpresiakas, A.; Sokos, E.; Doutsos, T. The tectonic setting and earthquake ground hazards of the 1993 Pyrgos earthquake, Peloponnese, Greece. *J. Geol. Soc. Lond.* **1996**, *153*, 39–49. [[CrossRef](#)]
69. Sabatakakis, N.; Koukis, G.; Mourtas, D. Composite landslides induced by heavy rainfalls in suburban areas: City of Patras and surrounding area, western Greece. *Landslides* **2005**, *2*, 202–211. [[CrossRef](#)]
70. Koukis, G.; Sabatakakis, N.; Ferentinou, M.; Lainas, S.; Alexiadou, X.; Panagopoulos, A. Landslide phenomena related to major fault tectonics: Rift zone of Corinth Gulf, Greece. *Bull. Eng. Geol. Environ.* **2009**, *68*, 215–229. [[CrossRef](#)]
71. Sabatakakis, N.; Koukis, G.; Vassiliades, E.; Lainas, S. Landslide susceptibility zonation in Greece. *Nat. Hazards* **2013**, *65*, 523–543. [[CrossRef](#)]
72. Kavoura, K. Landslide Hazard Model Evaluation in an Area of Western Greece. Ph.D. Thesis, University of Patras, Patras, Greece, 2017.
73. Kavoura, K.; Sabatakakis, N. Investigating landslide susceptibility procedures in Greece. *Landslides* **2020**, *17*, 127–145. [[CrossRef](#)]
74. Kordouli, M. Landslide Susceptibility Procedures Using Multi-Administration Systems. Ph.D. Thesis, University of Patras, Patras, Greece, 2020.
75. Cruden, D.M.; Varnes, D.J. Landslide types and processes. In *Landslides: Investigation and Mitigation*; Turner, A.K., Shuster, R.L., Eds.; Transportation Research Board Special Report; National Research Council: Washington, DC, USA, 1996; Volume 247, pp. 36–75.
76. Fell, R. Landslide Risk Assessment and Acceptable Risk. *Can. Geotech. J.* **1994**, *31*, 261–272. [[CrossRef](#)]
77. Gumbel, E.J. *Statistics of Extremes*; New York Chichester, West Sussex; Columbia University Press: New York, NY, USA, 1958.
78. Kottegoda, N.T.; Rosso, R. *Applied Statistics for Civil and Environmental Engineers*, 2nd ed.; Blackwell Publishing Ltd.: London, UK, 2007; pp. 295–305.
79. Chow, V.T.; Maidment, D.R.; Mays, L.W. *Applied Hydrology*; McGraw-Hill: New York, NY, USA, 1988; pp. 380–409.
80. Cislighi, A.; Cohen, D.; Gasser, E.; Bischetti, G.B.; Schwarz, M. Field measurements of passive earth forces in steep, shallow, landslide-prone areas. *J. Geophys. Res. Earth Surf.* **2019**, *124*, 838–866. [[CrossRef](#)]
81. Bischetti, G.B.; Di Fidio, M.; Florineth, F. On the origin of soil bioengineering. *Landsc. Res.* **2014**, *39*, 583–595. [[CrossRef](#)]
82. Bischetti, G.B.; De Cesare, G.; Mickovski, S.B.; Rauch, H.P.; Schwarz, M.; Stangl, R. Design and temporal issues in soil bioengineering structures for the stabilisation of shallow soil movements. *Ecol. Eng.* **2021**, *169*, 106309. [[CrossRef](#)]
83. Petrone, A.; Preti, F. Soil bioengineering for risk mitigation and environmental restoration in a humid tropical area. *Hydrol. Earth Syst. Sci.* **2010**, *14*, 239–250. [[CrossRef](#)]
84. Rey, F.; Bifulco, C.; Bischetti, G.B.; Bourrier, F.; De Cesare, G.; Florineth, F.; Graf, F.; Marden, M.; Mickovski, S.B.; Phillips, C.; et al. Soil and water bioengineering: Practice and research needs for reconciling natural hazard control and ecological restoration. *Sci. Total. Environ.* **2019**, *648*, 1210–1218. [[CrossRef](#)] [[PubMed](#)]